PREDICTION OF STRUCTURAL AND ELECTRONIC PROPERTIES OF Y-Ti-O COMPLEX OXIDES USING AB-INITIO CALCULATIONS—Y. Jiang, J. R. Smith, and G. R. Odette (University of California, Santa Barbara)

OBJECTIVE

The broad objective of this study is to develop a rigorous understanding of the fundamental character of the nm-scale Y-Ti-O enriched features (NFs) that impart high strength and radiation damage resistance to nanostructured ferritic alloys (NFAs) using ab inito density functional theory (DFT) calculations. The short-term objective, was to use DFT to model the crystal structural and electronic properties of the two major equilibrium Y-Ti complex oxide phases, as a baseline for examining non-equilibrium features.

SUMMARY

Our objective is to develop a fundamental understanding of the identity and character of nm-scale features (NFs) in nanostructured ferritic alloys (NFAs), especially at the smallest sizes. The NFs' features are believed to be responsible for the very high creep strength and radiation damage resistance of NFAs. Atom probe tomography studies have indicated that the NFs have Ti + Y to O ratios greater than 1 and Ti to Y ratios much greater than 1. These elemental ratios are inconsistent with the known complex oxide phases in the Ti-Y-O system, which include complex cubic pyrochlore $Y_2Ti_2O_7$ and orthorhombic (at lower temperatures) Y_2TiO_5. Both of these phases have been observed in transmission electron microscopy studies of NFAs, but generally in a size range that is larger than the smallest, and very likely, non-equilibrium NFs. There are also a number of other open questions including the basic thermokinetics of NF precipitation and coarsening; and the basic characteristics of NFs, such as elastic properties and interface structures, that mediate their interactions with dislocations. Since it is difficult, if not impossible, to fully address many of these questions with direct experimental measurements, we have developed a multiscale modeling approach that will complement a range of characterization techniques that are needed to obtain reliable answers.

As a starting point we have carried out first-principles DFT calculations for the equilibrium bulk phase $Y_2Ti_2O_7$ and Y_2TiO_5. The minimum 0°K energy, relaxed structure of these oxides was determined and used to calculate selected ground state properties, such as lattice constants, bulk modulus and internal structure parameters. Our results compare favorably with available experimental measurements and other first principles calculations. For example, the DFT calculations predict $Y_2Ti_2O_7$ has a higher bulk modulus than Fe, which is, in turn, higher than that for Y_2TiO_5. These moduli differences may influence the interactions of dislocations with oxide pinning features in a way that influences high temperature creep strength, for example, as mediated by detachment mechanisms. We also performed analysis of electron localization functions and densities of state to describe the nature of chemical bonding. It is found that although both oxides are highly ionic, the (Ti,Y)-O bonds contain some covalent character and that the Ti-O bonds have higher covalency than Y-O bonds.

PROGRESS AND STATUS

Introduction

Nanostructured ferritic alloys (NFAs) are being developed for use as high temperature structural materials, and they are especially promising for advanced fission and fusion energy applications [1,2]. NFAs contain a high number density of nm-scale clusters, or precipitates features (NFs), which provide creep resistance at elevated temperatures, as well as sites for annihilating radiation displacement damage and trapping of transmutation product helium. Small angle neutron scattering (SANS) and atom probe tomography (APT) studies have shown that the NFs are rich in Y, Ti, and O, but the measured (Ti + Y)/O and Ti/Y ratios are not consistent with known Y-TI-O equilibrium oxides, like $Y_2Ti_2O_7$ and Y_2TiO_5 [3,4]. However, transmission electron microscopy studies have observed both $Y_2Ti_2O_7$ and Y_2TiO_5 particles in NFAs, but generally at a larger size than the smallest NFs [5,6]. While the basic structures of the equilibrium oxides are well known, many of their other key characteristics are not understood. Thus

as a baseline for a larger longer-term effort, we have used ab-initio calculations to obtain better understanding of these bulk oxides through determination of atomic and electronic structures.

RESULTS

Structural Properties

$Y_2Ti_2O_7$ has a pyrochlore structure which has a high symmetry (space group, $Fd\overline{3}m$, O_h^7). Atoms are located at the following Wyckoff positions: Y at 16d (1/2, 1/2, 1/2), Ti at 16c (0, 0, 0), O at 48f (δ, 1/8, 1/8), and O' at 8b (3/8, 3/8, 3/8). The two non-equivalent oxygen sites, O and O', differ in chemical environment: each O resides in a Y + Ti-tetrahedron (defined by two Y and two Ti atoms), while each O' is in a Y-tetrahedron (defined solely by Y atoms). The displacement of each O-site due to the neighboring unoccupied Ti-tetrahedrons (defined solely by Ti atoms), δ, is the only internal structure parameter.

Figure 1a shows the pyrochlore lattice of $Y_2Ti_2O_7$ before structural relaxation. To optimize the structure, we used the DFT simulation package VASP [7]. DFT calculations were performed by using pseudo-potentials generated with the projector-augmented wave (PAW) method [8]. The semi-core 3p electrons of Ti and 4s and 4p of Y were all treated as valence electrons. The local density approximation (LDA) and the generalized gradient approximation (GGA-PW91 [9] and PBE [10]) were used to describe the exchange-correlation effects. For electron eigenvalues and Brillouin-Zone integrations, a uniform 4×4×4 Monkhorst-Pack k-mesh was used. During the structural relaxation, all force components converged within 0.01 eV/Å. Figure 1b shows the 1/8 corner of the conventional cell of $Y_2Ti_2O_7$ after structural relaxation/optimization.

Table 1 summarizes the results of our calculation compared to both those with those from a previous full-potential calculation [11] as well as experimental data [12]. The overall agreement is good. The discrepancies with the measured values on lattice constant are 0.89% (PW91), 1.09% (PBE) or -0.89% (LDA), respectively. The experimental bulk modulus has not been found. Our results deviate from the full-potential results by 0.69% (PW91), 0.89% (PBE) or -1.09% (LDA) in lattice constant and by -5.26% (PW91), -6.30% (PBE) or 8.17% (LDA) in bulk modulus, respectively. This trend is consistent with the general observation that GGA often overestimates the lattice constant and underestimates the bulk modulus, while LDA does the opposite. The theoretical $Y_2Ti_2O_7$ best estimate bulk modulus is ≈ 190±10 GPa. Our pseudo potential approach is fairly accurate, compared to the full-potential method, but is much more computationally efficient. The Ti-O bond length is calculated as 1.97 Å and the Y-O as 2.50 Å.

To the best of our knowledge, no theoretical calculations have been reported for α-Y_2TiO_5. The α-Y_2TiO_5 orthorhombic structure is stable under 1330°C, which is the temperature range of interest, transforming to the hexagonal β-Y_2TiO_5 between 1330°C and 1520°C and a fluorite-type phase at higher temperatures [13]. The orthorhombic α-Y_2TiO_5 has a complicated structure (with a space group of Pnma or D_{2h}^{16}). All atoms are in Wyckoff positions of 4c: (x, ¼, z), (-x+1/2, ¾, z+1/2), (-x, ¾, -z) and (x+1/2, ¼, -z+1/2), lying in the mirror planes at y=1/2 or ¾. The experimentally determined [14] internal structure parameters, x and z, for each atom were used to specify the initial positions for structural optimization. Figure 2 is the optimized crystal structure of α-Y_2TiO_5. Table 2 summarizes the calculated bulk properties using various methods that are compared to experimental structural data. No experimental data of bulk modulus has been found. The theoretical best estimate of the bulk modulus of α-Y_2TiO_5 is ≈ 130 ± 5 GPa. The optimized atomic coordination parameters are compared with experiment in Table 3. The five-coordinated Ti-O distances vary in the range of 1.79-1.97 Å, with an average of 1.89 Å (the same as the experimental value [14]). The seven-coordinated Y-O distances vary in the range of 2.28-2.38 (Y(1)-O) and 2.32-2.40 Å (Y(2)-O), with an average of 2.32 and 2.36 Å, respectively (compared with the experimental values of 2.32 and 2.35 Å [14])

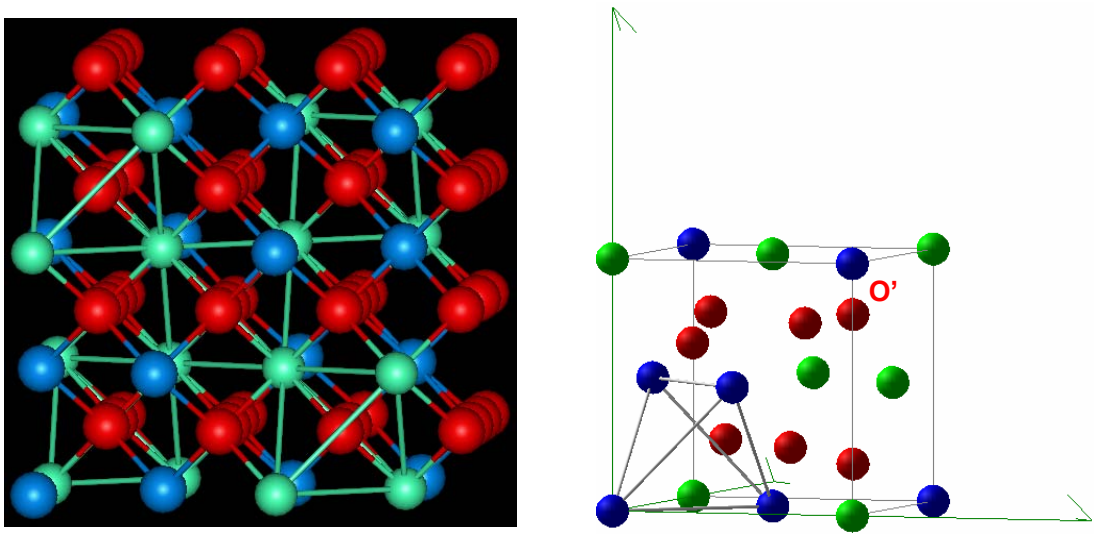

(a) (b)

Fig. 1. (a) The pyrochlore lattice of $Y_2Ti_2O_7$ before structural relaxation. Y, Ti and O atoms are represented in green, blue and red respectively. (b) The 1/8 corner of the conventional cell after relaxation. The Ti-tetrahedron is empty (free of oxygen) and located at the lower left corner. All O-sites displace by an amount of δ towards the neighboring Ti-tetrahedrons, while the O'-site (3/8, 3/8, 3/8) is unaffected.

Table 1. Calculated lattice constant, bulk modulus, internal structure parameter of $Y_2Ti_2O_7$, compared with previous theoretical and available experimental data

Method	Lattice Constant a (Å)	Bulk Modulus B (GPa)	Oxygen Displacement (δ)
PAW-LDA	10.0	208.76	0.330
PAW-PW91	10.18	182.85	0.329
PAW-PBE	10.20	180.84	0.329
FP-GGA [11]	10.11	193	0.329
Expt [12]	10.09	-	0.328

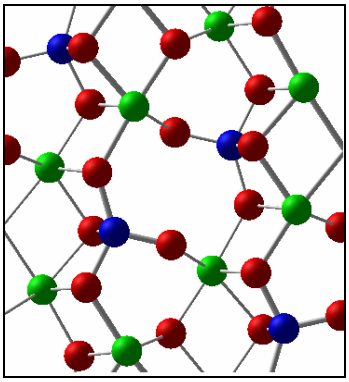

Fig. 2. The optimized crystal structure of α-Y_2TiO_5. The heavier bars represent bonds of atoms at y=3/4, the lighter at y=1/4 and between.

Table 2. Calculated lattice parameters of $Y_2Ti_2O_5$ compared with experiment. The experimental bulk modulus has not been found.

Method	Lattice Constant (Å)			Bulk Modulus B (GPa)
	a	B	c	
PAW-LDA	10.24	3.65	11.13	132.30
PAW-PW91	10.48	3.71	11.34	128.70
PAW-PBE	10.46	3.73	11.36	128.91
Expt[14]	10.35	3.7	11.25	-

Table 3. The calculated coordination parameters (using PAW-PW91) compared with experiment [14]

atom	Atomic Coordination Parameters (y=3/4)			
	Expt		Calc	
	x*	Z*	x	z
Y(1)	0.1156	0.2231	0.1150	0.2242
Y(2)	0.1366	0.5578	0.1361	0.5568
Ti	0.1745	0.8806	0.1738	0.8813
O(1)	0.4947	0.1024	0.4930	0.1046
O(2)	0.2229	0.0449	0.2232	0.0432
O(3)	0.2594	0.7340	0.2567	0.7306
O(4)	0.5085	0.6601	0.5070	0.6566
O(5)	0.2690	0.3833	0.2637	0.3841

The results of these first principles calculations of the bulk moduli of the complex oxides indicate that $Y_2Ti_2O_7$ (B ≈ 190 GPa) is stiffer than Fe (B ≈ 168 GPa [15]) and that $Y_2Ti_1O_5$ (G ≈ 130 GPa) is less stiff. Thus, to first order, it would be expected that dislocations would be repelled by incoherent $Y_2Ti_2O_7$ and attracted by incoherent Y_2TiO_5. Such differences could play a critical role in the relative effectiveness of these two phases in providing high temperature creep strength. Specifically, Y_2TiO_5 would be expected to provide more effective high temperature dislocation pinning since it would activate the detachment barrier mechanism. Of course the actual physics of high temperature creep strength is much more complex, but this example illustrated how materials by design approach to developing NFAs could be very powerful.

Electronic Properties

While the electronic properties of the oxides are not themselves of direct interest, they provide physical insight on the corresponding structural and physical properties. Electronic structure calculations are also of interest in interpreting experimental measurements based on techniques such as extended x-ray absorption spectroscopy (EXAFS). As shown in Fig. 3, the dimensionless electron localization function (ELF) that ranges from 0 to 1 [16] can be used to visualize the nature of the bonds in both oxides. High ELF values are typically associated with inert cores, covalent bonds or lone pairs. The ELF value is high at each ion and is small, but not zero, in between, suggesting some covalent character of the dominantly ionic bonds. The Ti-O bonds appear to be somewhat more covalent than the Y-O bonds.

To be more quantitative, we computed the electron density of states (DOS) for both oxides using the tetrahedron method [17]. The site- and lm-projected DOS are shown in Fig. 4. The valence bands are largely composed of O-2p and (Y,Ti)-d states, and the unoccupied conduction bands by a mixing of Ti-3d and Y-4d states. The calculated band gaps are 2.84 and 3.14 eV for $Y_2Ti_2O_7$ and Y_2TiO_5, respectively.

The stronger hybridization of (Ti-3d, O-2p) than that of (Y-4d, O-2p) is evident in both oxides. This is associated with the shorter Ti-O bond length than the Y-O in both oxides. The Ti-3d states interact with the O-2p over a wider energy range in $Y_2Ti_2O_7$ than in Y_2TiO_5, but the difference is small. Due to their different structural surrounding, differences in the (Ti,Y)-O interactions do not directly explain the difference of elastic moduli in the two oxides. Indeed, each Ti (or Y) is coordinated with six (or eight) O ions in $Y_2Ti_2O_7$, while in Y_2TiO_5 each Ti (or Y) is coordinated with five (or seven) O. The different coordination numbers are also responsible for the difference in bond lengths: the bond lengths of (Ti,Y)-O in $Y_2Ti_2O_7$ are even larger than in Y_2TiO_5 by 4~6%, even though the former has a higher predicted bulk modulus.

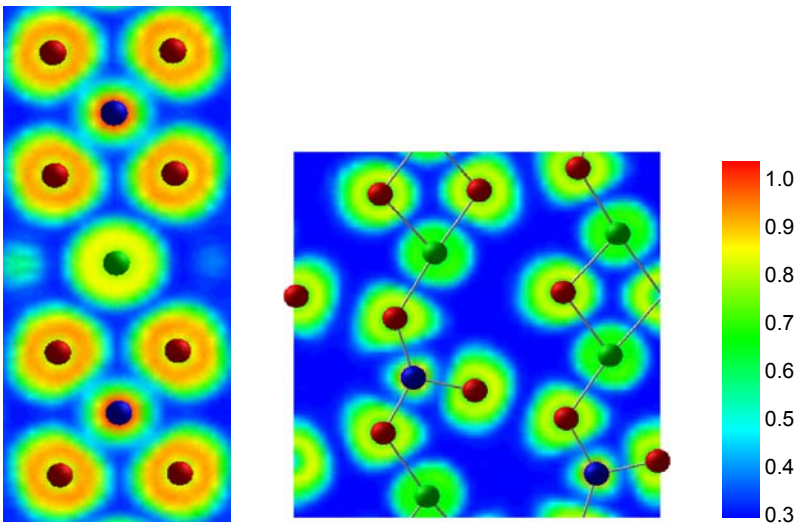

Fig. 3. ELF plots showing the degree of covalency of the (Ti,Y)-O bonds in both (a) $Y_2Ti_2O_7$ and (b) Y_2TiO_5. The $Y_2Ti_2O_7$ plot is at about 10 degree tilt from the (111) plane, in order to present both Y-O and Ti-O bonds in the same plane, while the plot of Y_2TiO_5 right is at y=3/4.

Future Work

The results reported here represent the beginning phase of a longer term, broader effort to understand and model the basic characteristics and thermokinetics of a range of NFs that form in NFAs. Future work will extend the first principles models to treat finite temperature effects on both physical (e.g., elastic) and thermodynamic (e.g., elemental and (Y,Ti)-0 complex activities) properties of various possible phases (including non-equilibrium atom positions and structures), interfaces (including diffuse and segregated/chemically partitioned structures) and diffusion coefficients.

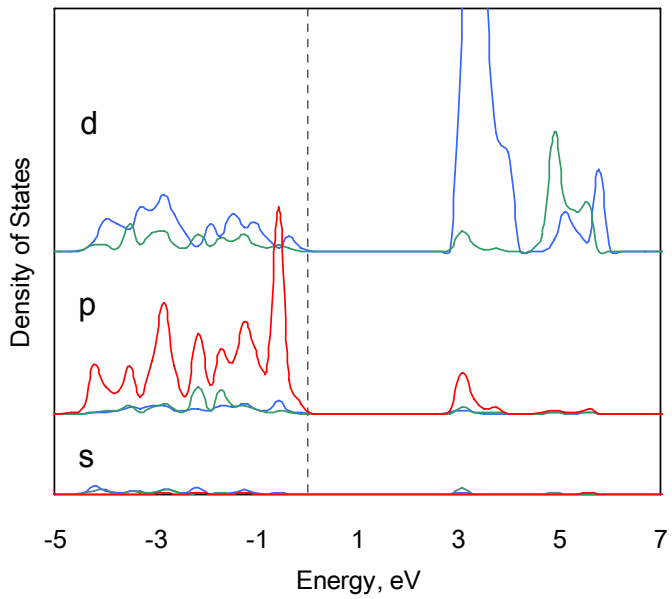

(a)

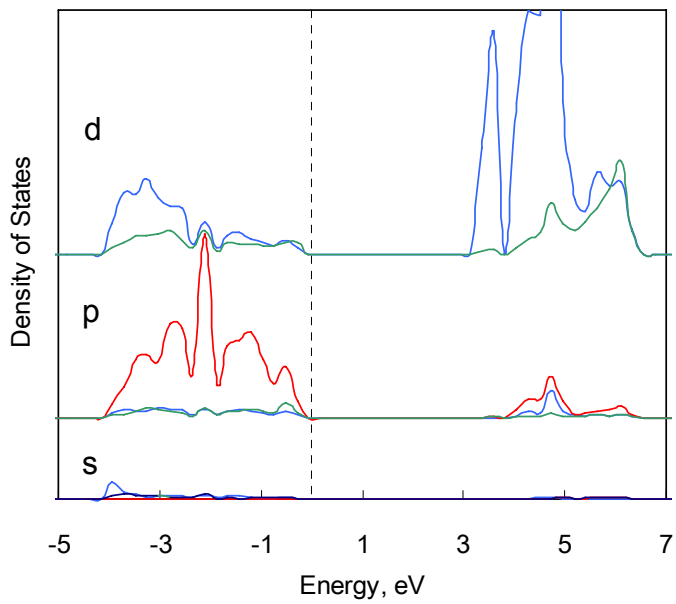

(b)

Fig. 4. Calculated site-projected partial DOS of (a) $Y_2Ti_2O_7$ and (b) Y_2TiO_5. Blue, green, and red solid lines represent Ti, Y, and O sites respectively. The vertical dotted line denotes the valence band maximum.

REFERENCES

[1] M. J. Alinger, G. R. Odette, and D. T. Hoelzer, J. Nucl. Mater. 329–333 (2004) 382.
[2] S. Ukai and M. Fujiwara, J. Nucl. Mater. 307–311 (2002) 749.
[3] H. Kishimoto, M. J. Alinger, G. R. Odette, and T. Yamamoto, J. Nucl. Mater. 329–333 (2004) 369.
[4] M. K. Miller, E. A. Kenik, K. F. Russell, L. Heatherly, D. T. Hoelzer, and P. J. Maziasz, Mater. Sci. Eng. A353 (2003) 140; see also M. K. Miller, D. T. Hoelzer, E. A. Kenik, and K. F. Russell, Microsc. Microanal. 10 (Suppl. 2) (2004) 708.
[5] S. Yamashita, S. Ohtsuka, N. Akasaka, S. Ukai, and S. Ohnukiy, Philos. Mag. Lett. 84 (2004) 525.

[6] M. Klimiankou, R. Lindau, and A. Moslang, J. Nucl. Mater. 329–333 (2004) 347.
[7] G. Kresse and J. Furthmüller, http://cms.mpi.univie.ac.at/vasp/vasp/vasp.html.
[8] G. Kresse and J. Joubert, Phys. Rev. B 59 (1999) 1758.
[9] J. P. Perdew, in P. Ziesche and H. Eschrig (eds.), Electronic Structure of Solids '91 (Akademie Verlag, Berlin, 1991) 11.
[10] J. P. Perdew, K. Burke, and M. Ernzerhof, Phys. Rev. Lett. 77 (1996) 3865.
[11] R. Terkia, G. Bertranda, H. Aouragb, and C. Coddet, Physica B 392 (2007) 341.
[12] M. A. Subramanian, G. Aramudan, and G. V. Subba Rao, Prog. Solid State Chem. 15 (1983) 55.
[13] N. Mizutani, Y. Tajima, and M. Kato, J. Am. Ceram. Soc. 59 (1976) 168.
[14] W. G. Mumme and A. D. Wadsley, Acta Crystallogr. B24 (1968) 1327.
[15] C. Kittel, Introduction to Solid State Physics, 6th Ed. (John Wiley, New York, 1986) 23, 55, 57.
[16] A. D. Becke and K. E. Edgecornbe, J. Chem. Phys. 92 (1990) 5397.
[17] P. E. Blochl, O. Jepsen, and O. K. Andersen, Phys. Rev. B 49 (1994) 16223.